

1 **On seismicity and structural style of oceanic transform**
2 **faults: a field geological perspective from the Troodos**
3 **ophiolite, Cyprus**

4

5 Åke Fagereng and Christopher J. MacLeod

6

7 *School of Earth & Ocean Sciences, Cardiff University, Park Place, CF10 3AT, Cardiff,*
8 *United Kingdom*

9

10

11 *Manuscript submitted to ‘Transform Plate Boundaries and Fracture Zones’, and an*
12 *edited, proofed, and typeset version was published by Elsevier, September 2018 as:*

13

14 Fagereng, Å. and MacLeod, C.J., 2019. On Seismicity and Structural Style of Oceanic
15 Transform Faults: A Field Geological Perspective From the Troodos Ophiolite,
16 Cyprus. In *Transform Plate Boundaries and Fracture Zones* (pp. 437-459). Elsevier.

17

18

19

20

21

22

23

24

25

26

27

28

29

30

31

32

33

34 **ABSTRACT**

35 Aseismic creep accommodates the majority of displacement along active oceanic
36 transform faults, also within their thermally defined seismogenic zone. The significant
37 earthquakes that do occur are near periodic, and repeat in nearly constant locations.
38 Neither of these observations is explained by current models that infer an olivine-
39 dominated rheology and a thermally controlled seismogenic zone. In this contribution
40 we review geological observations from the exhumed Southern Troodos Transform
41 Fault Zone of Cyprus, and discuss their implications for seismogenesis at modern
42 oceanic transform faults. In crustal level rocks, displacement was accommodated on
43 discrete faults and in broad breccia zones, whereas at mantle levels the dominant
44 structures are serpentinite mélanges overprinting rare and volumetrically minor,
45 ductilely deformed peridotites. We speculate that the seismic style of crustal level
46 faults depends on whether slip is localised, or distributed over a broad zone that must
47 dilate during shear. At mantle levels, we highlight that the dominant deforming
48 material is serpentinite, at least when – as in the case of Troodos – sufficient hydration
49 has taken place. Our observations and inferences imply that transform fault seismicity
50 depends on time- and strain- and permeability-dependent processes, and is governed by
51 geological complexity at a range of scales.

52

53 **INTRODUCTION**

54 Oceanic transform fault plate boundaries may offset mid-ocean ridges by
55 hundreds of kilometres. Because earthquake moment magnitude (M_w) normally scales
56 with rupture length (Wells and Coppersmith, 1994), oceanic transform faults should
57 therefore produce many great to giant earthquakes. However, it has long been
58 recognised (e.g. Brune, 1968; Bird et al., 2002) that oceanic transforms host fewer, and
59 smaller, earthquakes than predicted by magnitude-length relationships. Consequently,
60 it has been suggested that most displacement on transform faults is accommodated by
61 aseismic creep, accompanied by microseismicity of insignificant cumulative moment
62 (Boettcher and Jordan, 2004). Where larger earthquakes ($M_w \geq 6.0$) do occur, they
63 tend to repeat quasi-periodically on persistent locked fault patches (McGuire et al.,
64 2005; Braunmiller and Nábělek, 2008; Sykes and Ekström, 2012). A picture is
65 therefore emerging where oceanic transforms, although commonly considered
66 lithologically and rheologically simple, appear to have a more complicated internal
67 structure comprising locked asperities within larger, creeping regions.

68 To a first order the down-dip limit of transform fault seismogenesis is generally
69 well approximated by a thermally controlled, frictional-viscous transition in olivine-
70 rich rocks along the 600°C isotherm, assuming a simple half-space cooling model
71 (McKenzie et al., 2005; Boettcher et al., 2007; Braunmiller and Nábělek, 2008).
72 However, in detail there are problems with this inference; for example, the
73 predominantly aseismic behaviour at temperatures less than 600°C is not consistent
74 with the observed velocity-weakening behaviour of olivine-dominated rocks deformed
75 in the laboratory under these conditions (Boettcher et al., 2007). A thermal control on
76 earthquake distribution is also inconsistent with significant, along-strike variation in
77 focal depths (Abercrombie and Ekström, 2001; McGuire et al., 2012), although
78 numerical models that incorporate hydrothermal cooling can explain some
79 observations of deeper seismicity (Roland et al. 2010). One hypothesis for steady-state
80 aseismic behaviour cooler than the 600°C isotherm is that hydration and alteration of
81 olivine to serpentine causes velocity-strengthening slip under some conditions (Reinen
82 et al., 1991; Moore et al., 1997; Boettcher and Jordan, 2004). Other possibilities
83 involve the effects of fluid pressure to lower effective normal stress and enable
84 velocity-strengthening creep (Scholz, 1998), or else that spatially variable degrees of
85 damage may lead to heterogeneous fluid-mechanical rock properties (Roland et al.,
86 2012; Froment et al., 2014).

87 To date, discussion on the seismic behaviour of transform faults has been based
88 upon a combination of remote and ocean floor seismological observations, inferences
89 drawn from laboratory experiments, and numerical models. Direct sampling, mostly by
90 dredging, has informed the debate to only a limited extent (e.g. Prinz et al., 1976;
91 Honnorez et al., 1984). None of the above data sets can capture the nature or scale of
92 geological variability, in 3-D, that must explain the complex and heterogeneous
93 seismic style observed along oceanic transforms. To address this knowledge gap we
94 consider the variability in lithology and deformation style that has been documented
95 along the Southern Troodos Transform Fault Zone, a late Cretaceous oceanic transform
96 fault preserved within the exhumed Troodos ophiolite of Cyprus (MacLeod and
97 Murton, 1993; Gass et al., 1994). This ~5 km wide seafloor fault zone exposes a
98 complexly-deformed section of mantle to oceanic crustal rocks deformed at
99 temperatures from > 1000°C down to ambient, preserved following uplift and erosion
100 of the ~90 Myr old ophiolite massif. We briefly review the questions posed by
101 geophysical observations along well-studied oceanic transforms, and critically evaluate

102 associated geological models for fault zone structure in the light of our observations
103 from the Troodos ophiolite.

104

105 **SEISMIC COUPLING OF ACTIVE TRANSFORMS**

106 The seismic coupling coefficient, χ , describes the fraction of plate motion,
107 within the crustal seismogenic zone, that is accommodated seismically. Note that this
108 use of the term ‘coupling’ differs from a classic use describing transmission of stresses
109 across a fault – in this chapter, there is no inference of a direct link between degree of
110 coupling and stress on a fault plane (cf. Wang and Dixon, 2004). A typical definition
111 of seismic coupling is $\chi = \Sigma M_{\text{obs}} / \Sigma M_{\text{ref}}$ (Scholz, 2002), where ΣM_{obs} and ΣM_{ref} are the
112 sums of observed and expected seismic moment, respectively. Seismic moment is
113 defined as $M = GAu$, where G is shear modulus, A is rupture area, and u is average
114 slip, and relates to earthquake magnitude by the relation: $M_w = (2/3) \log_{10} M - 6$ where
115 M is measured in Nm. Typically, faults are considered as comprising areas that are
116 either creeping ($\chi = 0$) or locked and hosting episodic earthquake slip ($\chi = 1$), so that a
117 seismic coupling of $0 < \chi < 1$ implies that some portions of the fault are locked while
118 others creep. Making the assumption that the base of the seismogenic zone is
119 controlled by the 600°C isotherm, Boettcher and Jordan (2004) estimated a global χ for
120 oceanic transforms of 0.15 ± 0.02 , in other words that only 15 % of transform
121 displacement occurs seismically.

122 The dearth of seismicity on oceanic transforms was first recognized by Brune
123 (1968), who envisaged this observation as arising from a relatively small effective
124 seismogenic thickness – defining ‘seismogenic’ as zones where earthquakes nucleate.
125 However, this model of a fully coupled depth interval requires a seismogenic zone that
126 is less than a kilometre thick (Bird and Kagan, 2004), and is consistent neither with the
127 observed depth distribution of earthquake hypocentres throughout the oceanic crust
128 and into the upper mantle (Abercrombie and Ekström, 2001; McGuire et al., 2012), nor
129 with the rupture dimensions of large transform fault earthquakes (Abercrombie and
130 Ekström, 2001). An alternative model is that the seismogenic zone has greater down-
131 dip extent than the statistically determined effective seismogenic thickness, but is
132 laterally discontinuous (Boettcher and Jordan, 2004); in other words, transforms may
133 be regarded as comprising small seismogenic patches within predominantly aseismic
134 faults, similar to models for predominantly creeping subduction thrusts in the ‘asperity
135 model’ of Lay and Kanamori (1981).

136 In an example of coupling within single transform systems, Braunmiller and
137 Nábělek (2008) report $\chi \sim 0.25$ on the Blanco Transform, which connects the Gorda
138 and Juan de Fuca ridges in the North Pacific. Here, long, straight, mature segments are
139 largely coupled, whereas immature fault systems are wider, more complex, and have
140 lower degree of coupling. In comparison, the south Pacific Eltanin transform has $\chi \sim$
141 0.1 (Stewart and Okal, 1983), and comprises three, dominantly aseismic, *en echelon*
142 faults containing locked zones hosting quasi-periodic events of $M_w \leq 6.4$ (Molnar et
143 al., 1975; Sykes and Ekström, 2012). Rupture size appears determined by segment
144 length, and an inferred 5 km deep base to the seismogenic zone (Sykes and Ekström,
145 2012), limiting the maximum seismic moment by limiting rupture area. Both of these
146 examples are consistent with locked, seismogenic, patches embedded in dominantly
147 creeping fault zones. These locked zones are persistent, and thus, there may be
148 connections between χ and fault maturity, geometry, or material properties, but the
149 geological nature of locked vs. creeping fault segments is not well constrained.

150

151 **OBSERVATIONS FROM ACTIVE TRANSFORM FAULTS**

152 In most instances individual transform faults are not simply composed of a
153 single continuous lineament connecting two spreading ridge tips. A typical geometry
154 may instead involve more than one continuous transform lineament, relayed by
155 transtensional basins or transpressional push-ups, within a morphologically complex
156 valley that may be >5 km wide (e.g. Searle, 1981; 1983; Fox and Gallo, 1984;
157 Macdonald, 1986; Pockalny et al., 1988; Embley and Wilson, 1992). Intra-transform
158 magmatism may occur (e.g. Hékinian et al., 1995). Transform valleys may be bordered
159 by detachment faults or transverse ridges (e.g. Bonatti and Honnorez, 1976; Karson
160 and Dick, 1983). Thermally generated bending stresses play a major role in generating
161 topographic relief within and across transform valleys (Wessel and Haxby, 1990).

162 Detailed microseismic observations along some well-studied oceanic
163 transforms illustrate their heterogeneity and have led to a number of conceptual models
164 for transform fault seismic style (Figure 1). Along the East Pacific Rise, M_w 6
165 transform earthquakes repeat at 5 to 6-year intervals in persistent locked patches
166 (McGuire et al., 2005) (Figure 1a). In western Gofar, McGuire et al. (2012) located $>$
167 20,000 microearthquakes during an ocean bottom seismometer deployment. They
168 found that areas between locked patches host intense foreshock sequences involving
169 thousands of microearthquakes, with depths extending a few kilometres into the upper

170 mantle. The $6.0 \leq M_w \leq 6.2$ mainshocks, on the other hand, are confined to the crust
171 and propagate neither into surrounding microseismically active, creeping regions, nor
172 into the upper mantle. On the Discovery transform fault, also on the East Pacific Rise,
173 interseismically locked patches also fail repeatedly in M_w 6.0 earthquakes constrained
174 to the crust (McGuire, 2008) separated by microseismically active, dominantly
175 aseismic zones ≤ 10 km long (Wolfson-Schwehr et al., 2014). The observations on the
176 East Pacific Rise are consistent with ‘single-mode’ behaviour (Figure 1b), where fully
177 locked fault patches fail in seismic events of predictable regularity, with little to no co-
178 seismic rupture of interseismically creeping, but microseismically active surrounding
179 material (McGuire et al., 2005; 2012).

180 The geological reasons for the bimodal seismic style along the East Pacific Rise
181 are unclear. Fault bends of a few kilometres have been observed to arrest propagating
182 M_w 6 earthquakes in continental transforms (Wesnousky, 2006). Froment et al. (2014)
183 report a ~ 600 m bend in the Gofar transform at the boundary between the locked patch
184 and the foreshock zone (Figure 1a), representing a much smaller geometrical
185 irregularity than those arresting ruptures in the continents. Therefore, these authors
186 interpret this bend to reflect an along-strike change in mechanical properties, rather
187 than represent a geometrical rupture barrier. The nature of this variation in properties is
188 an open question. A microseismically active creeping zone has anomalously low P-
189 wave velocity, which could be explained by high porosity and increased pore fluid
190 pressure (Roland et al., 2012). In this case, it is therefore possible that the foreshock
191 zone prevents rupture propagation through dilatant hardening as the rupture front hits
192 the high porosity rocks (Segall et al., 2010), and/or because aseismic slow-sliding of
193 fluid-overpressured fault rocks prevents the elastic loading required for seismic slip
194 (Segall and Rice, 1995). The S-wave velocity of the creeping zone temporarily
195 decreased during a foreshock sequence (McGuire et al., 2012; Froment et al., 2014),
196 interpreted as increased damage, possibly by aseismic deformation accompanying the
197 microseismic foreshocks (McGuire et al., 2012).

198 Repeating sequences are also observed along the northern Mid-Atlantic Ridge,
199 where slip rates are lower (Figure 1c). On the Charlie-Gibbs Transform, a M_w 7.1
200 earthquake in 2015 occurred at approximately the same epicentral location as a 1974
201 earthquake of similar magnitude, and similarly a 1998 M_w 6.8 event appears to repeat
202 an event observed in 1967 (Aderhold and Abercrombie, 2016). The repeating rupture
203 patches are not separated by any distinct geometrical barriers (Figure 1c), indicating

204 these may also relate to along-strike variation in fault zone properties. The larger
205 magnitudes of these events relative to repeating events on the faster Gofar-Discovery
206 transform is consistent with a scaling relation where the maximum magnitude is
207 proportional to $V^{3/8}$ if V is time-averaged fault slip rate (Boettcher and Jordan, 2004).
208 Aderhold and Abercrombie (2016) calculate that χ may be as high as 0.88 for this fault,
209 if segments creeping in the interseismic period also accommodate some co-seismic
210 displacement. This is consistent with serpentinised zones sliding stably at plate tectonic
211 rates but become velocity-weakening at higher velocity (Reinen et al., 1994). Contrary
212 to the 'single mode' model of persistent locked and creeping zones, this 'multi-mode
213 model' (cf. Boettcher and Jordan, 2004) implies that the same area on a fault can
214 accommodate both creep and seismic slip; i.e. locked zones are surrounded by
215 conditionally stable materials that become velocity-weakening at elevated velocity
216 (Figure 1d). Such time-dependent behaviour has also been observed on subduction
217 thrusts (Zweck et al., 2002; Simons et al., 2011; Ide et al., 2011), and may arise from a
218 velocity-dependence of friction (Dieterich, 1992), dynamic weakening by thermal
219 pressurisation (Noda and Lapusta, 2013), or the behaviour of a tabular fault zone where
220 a range of materials of diverse rheological/frictional properties are intermingled
221 (Fagereng and Sibson, 2010; Collettini et al., 2011).

222 From the brief review presented here it is clear that many significant questions
223 remain as to the mechanical properties and seismic behaviour of oceanic transform
224 faults. It is evident that our knowledge of their physical properties far outstrips our
225 understanding of the geological controls on their behaviour.

226

227 **GEOLOGICAL SETTING OF THE SOUTHERN TROODOS TRANSFORM** 228 **FAULT ZONE**

229 Because of the difficulty of accessing the material that is being deformed in
230 modern oceanic transform fault zones it will always be difficult to provide the
231 geological ground-truthing necessary to answer the questions outlined above. An
232 alternative approach to gaining insight into transform fault mechanics from a
233 geological perspective is to examine a transform system preserved within exhumed
234 ocean floor. To our knowledge the best such example lies within the Troodos ophiolite
235 of Cyprus.

236 The Troodos ophiolite was formed by seafloor spreading in a small supra-
237 subduction zone ocean basin in the Late Cretaceous (Mukasa and Ludden, 1987;

238 Robertson et al., 2012). After formation this fragment of oceanic lithosphere
239 experienced $\sim 90^\circ$ of anticlockwise rotation in the latest Cretaceous (Morris et al.,
240 1990), before being underthrust and passively uplifted in the Miocene (Robertson et
241 al., 2012). Differential uplift and preferential erosion has led to mantle rocks being
242 exposed at the highest elevations, with progressively shallower stratigraphic units
243 exposed at lower elevations in a simple radial pattern dipping away from Mt Olympus
244 (Figure 2; Gass and Masson-Smith, 1963). Apart from this overall, large scale, dome
245 structure, the ophiolite is largely intact, free of metamorphic overprint, and allows field
246 study of all stratigraphic levels.

247 In marked contrast to the relatively simple domal structure of the main part of
248 the Troodos ophiolite, the southern margin shows significant small-scale complexity in
249 its outcrop pattern. This portion of the Troodos ophiolite, the 400 km² Limassol Forest
250 Complex and adjoining Arakapas Fault Belt (Figure 2), is notable for the presence of a
251 major ocean-floor strike-slip fault zone. At least 5 km in width and traceable for ~ 60
252 km along strike, this E-W trending fault zone is perpendicular to the overall N-S mean
253 sheeted dyke orientation in the main part of the ophiolite (e.g. Gass et al., 1994).
254 Overlain by undeformed ocean-floor sediments, it is generally accepted as being a
255 fragment of an oceanic transform fault zone that was preserved within the ophiolite
256 upon its exhumation (Moores and Vine, 1971; Simonian and Gass, 1978; Murton,
257 1986a; MacLeod, 1990; Gass et al., 1994). This seafloor structure has been termed the
258 ‘Southern Troodos Transform Fault Zone’ (STTFZ) (MacLeod, 1990; Gass et al.,
259 1994). After some debate it is now recognised as having been a dextrally-slipping
260 structure (MacLeod and Murton, 1995).

261

262 **GEOMETRY OF THE STTFZ**

263 The Arakapas Fault Belt (AFB) is a 0.5-1.5 km wide E-W trending zone of
264 intense dextral transcurrent faulting that separates the Limassol Forest Complex (LFC)
265 from the main Troodos ophiolite and marks the northern margin of the STTFZ (Figure
266 3; Simonian and Gass, 1978, Gass et al., 1994). It forms a marked valley today that is
267 inferred to mimic the original bathymetric depression coincident with the transform
268 fault zone (Simonian and Gass, 1978). Within the AFB, discrete braided cataclastic
269 fault strands separate blocks of extensively brecciated sheeted dyke complex (SDC).
270 Irregular sequences of lava flows, intercalated with volcanoclastic sediments, lie
271 unconformably on the SDC and fill small basins between upstanding fault blocks.

272 These sediments are highly variable in thickness, to a maximum of ~300 m. They are
273 dominated by mass flow breccia deposits intercalated with lava and dyke-derived
274 clasts, finer turbiditic sequences, and ferruginous hydrothermal sediment. These
275 observations are consistent with sediments derived by submarine erosion of fault
276 scarps within and on the flanks of the transform fault zone. They provide evidence for
277 local highs and lows within the transform valley at the time of deformation, but not
278 sufficient to expose the mantle on the seafloor, at least within the preserved AFB.

279 The nature of the extrusive sequence in the AFB contrasts markedly with the
280 orderly lava successions from the main Troodos ophiolite, in which volcanoclastic
281 sediments are extremely rare. Extrusives from the AFB and LFC are highly depleted
282 boninites derived from an extensive suite of syn-kinematic 'transform sequence'
283 wehrlite and gabbro plutons and associated dykes intruded into the LFC mantle
284 lithosphere (Murton 1986a; Gass et al., 1994). This intra-transform magmatism
285 provides evidence that the STTFZ was at least locally transtensional during its active
286 transform phase (Murton 1986a; MacLeod and Murton, 1993, 1995).

287 The present-day outcrop pattern of the LFC, to the south of the AFB, is far
288 more complicated geologically, with extensive exposures of serpentinised mantle
289 peridotites in the west and, to a lesser extent, in the northeast corner (Figure 3).
290 Widespread transform-related deformation of the mantle section is described in the
291 section below. Faulted blocks of plutonic rocks and SDC comprise much of the
292 remainder of the central LFC, with extrusives preserved around its periphery (Gass et
293 al., 1994). This complex disposition of outcrop reflects, in part, late Cretaceous and
294 Tertiary uplift and exhumation of the LFC; however, 1:5000 scale geological mapping
295 of the entire southern Troodos region (Figure 3; Simonian, 1975; Murton, 1986b;
296 MacLeod, 1988; Gass et al., 1994) has allowed the uplift history to be carefully
297 deconvolved from earlier active transform fault processes, as documented in detail
298 elsewhere (Murton, 1986a; MacLeod, 1990; MacLeod and Murton, 1993; Gass et al.,
299 1994). In summary, NE-SW stretching (in present coordinates) at the latest stage of its
300 ocean-floor history put the STTFZ into transtension; this led to extensional reactivation
301 of transform-parallel structures above a Moho-level detachment fault within the
302 STTFZ (MacLeod, 1990). Subsequently, the LFC massif underwent differential uplift
303 with respect to the main Troodos massif in response to subduction-related
304 underthrusting in the Miocene (e.g. Gass et al., 1994; Robertson et al., 2012). This is

305 manifested by reverse faults at the margins of the western LFC serpentinised peridotite
306 body.

307 A southern margin to the STTFZ was recognised in the eastern LFC by
308 MacLeod (1990), on the basis of the disappearance of interlava sediments in the
309 extrusive section and absence of originally E-W steep structures once later tilting had
310 been accounted for (Figure 3). This constrains the original width of the STTFZ to have
311 been approximately 5 km. We prefer this figure to the slightly greater estimate of
312 Murton (1986b), from the western LFC, which was made in the area complicated by
313 Miocene thrusting. Within the southeastern corner of the LFC, south of the margin of
314 the STTFZ, lies a domain of relatively regular axis-generated ocean crust apparently
315 unaffected by transform deformation (Figure 3). This region must, by inference, have
316 been formed at an 'Anti-Troodos' spreading axis on the opposite side of the STTFZ
317 from the main Troodos complex. Most or all of the regular crustal section exposed in
318 the LFC is inferred to have formed at the tip of the Anti-Troodos spreading axis and to
319 have become incorporated into the transform-tectonised zone.

320 Dyke and fault strikes within both the Anti-Troodos domain and main Troodos
321 massif are NE-SW (Figure 2, 3). Those to the north of the transform bend back to a N-
322 S overall trend typical of Troodos as a whole (Figure 2). This swing of dyke and fault
323 orientation mimics that of many modern oceanic transforms, at which ridge tips curve
324 towards the active transform zone as a result of the local rotation of the extensional
325 stress field (Figure 1a,c). On this basis some authors inferred sinistral movement on the
326 transform (e.g. Moores et al., 1990; Cann et al., 2001). This however conflicts with
327 direct geological evidence for dextral shear (MacLeod and Murton, 1995), and for
328 palaeomagnetic studies which documented significant clockwise vertical-axis tectonic
329 rotations in the NE-SW trending dyke domain (Bonhommet et al., 1988; Allerton and
330 Vine, 1990; MacLeod et al., 1990; Morris et al., 1990; Gass et al., 1994). MacLeod et
331 al. (1990) interpreted the spatial extent of the dyke swing, combined with evidence for
332 seafloor graben formation in the Solea region (Varga and Moores, 1985; Moores et al.,
333 1990), to show a preserved ridge-transform intersection west and north of the LFC
334 (Figure 2). They showed that dyke rotation does not markedly increase with distance
335 from the ridge-transform intersection, implying an early stage of distributed, rotational
336 deformation in young weak lithosphere near the ridge, and localisation onto the main
337 strike-slip STTFZ further from the ridge-transform intersection.

338 Palaeomagnetic studies from within the STTFZ itself are more limited than
339 those to the north and south, but a reconnaissance study reported in Gass et al. (1994)
340 found extreme clockwise rotations of $\geq 150^\circ$ about steeply plunging axes in the SDC.
341 Much of the SDC within the STTFZ is intensely brecciated and coherent areas with
342 identifiable dyke margins are small (metres to tens of metres) and relatively rare (see
343 below), hence it can be deduced that the sizes of rotating blocks were small compared
344 to the deforming zone as a whole (tens to hundreds of metres). Supporting evidence
345 that significant syn-magmatic rotational deformation is extensive within the active
346 transform fault zone comes from cross-cutting sheeted dyke swarms and from
347 transform sequence boninitic dykes intruded into the STTFZ. These show a range of
348 orientations, from N-S to NE-SW to E-W, often cross-cutting but with a consistent
349 anticlockwise younging sense (Murton, 1986a; MacLeod and Murton, 1993, 1995;
350 Gass et al., 1994). MacLeod and Murton (1995) suggested that transform sequence
351 gabbros were intruded at the margins of small (probably 100s of metres to km-sized)
352 blocks rotating independently within the broader (~5 km-wide) STTFZ.

353

354 **TRANSFORM FAULT ROCKS**

355 The differential uplift and erosion that has affected the LFC and AFB in the 90
356 Myr since the formation of the Troodos ophiolite allows access to all structural levels
357 of the original STTFZ and a unique opportunity to examine transform fault
358 deformation mechanisms in space and time from the original seafloor down to the
359 mantle lithosphere. We find that different lithologies and stratigraphic levels deform by
360 profoundly different mechanisms. In this section we describe the observed fault rock
361 types in order of inferred decreasing temperature and from deepest to shallowest.

362

363 ***High-temperature ductile deformation in the mantle sequence***

364 Mantle sequence peridotites in the western LFC are harzburgites with
365 subsidiary dunite bands/lenses. In the northeastern LFC massive dunite up to 200 m
366 thick predominates, taken to represent part of the mantle-crust transition zone (Gass et
367 al., 1994). Serpentinisation is near pervasive across the entire LFC, and generally
368 obscures or destroys the original textures in the peridotites. Where well preserved the
369 harzburgites display weak *l-s* tectonite fabrics defined macroscopically by the
370 preferred alignment of bastite pseudomorphs after orthopyroxene or, in some instances,
371 by chrome spinel, and/or cm-dm scale variation in the proportion of the pyroxene. In

372 rare instances, equigranular to mosaic porphyroclastic textures are preserved in thin
373 section. These high-temperature crystal-plastic fabrics are conventionally interpreted as
374 having formed by solid-state viscous flow in the convecting asthenosphere, then
375 passively frozen in during formation of the mantle lithosphere (e.g. Nicolas and
376 Poirier, 1976; Murton, 1986a; Gass et al., 1994). The orientations of these
377 'asthenospheric' fabrics are variable: generally NE-trending in the western LFC and
378 NW-trending in the northeastern LFC (Gass et al., 1994).

379 Steeply dipping, E-W striking planar fabrics, which would be parallel to the
380 transform fault as a whole, are only observed in a few places; dominantly in the
381 northernmost western LFC (Gass et al., 1994). In these instances, localised foliations
382 are relatively intense across widths of several decimetres (Figure 4a), within shear
383 zones that have been traced for metres to tens of metres (Murton, 1986a; Gass et al.,
384 1994). Lineations are rarely observed, likely because of poor exposure. Although no
385 microstructural studies have been possible because of the subsequent serpentinisation,
386 we presume these fabrics to pseudomorph porphyroclastic textures from localised
387 shear zones in the original peridotite. They are perhaps similar to the 'lithospheric'
388 shear zones described from the Oman ophiolite (Ceuleneer et al., 1988). These
389 'lithospheric' shear zones are rare, or rarely preserved, but are important as they
390 represent highest temperature deformation structures that can be related to transform
391 fault activity within the LFC. It should be emphasised that no porphyroclastic
392 peridotite mylonites with preserved, dynamically recrystallized matrix comparable to
393 those reported elsewhere (e.g. Warren and Hirth, 2006) have been reported from the
394 LFC. Although because of the subsequent serpentinisation and serpentinite
395 deformation (see below) it is difficult to determine the original extent of the high
396 temperature ductile shear zones, it is nevertheless evident that such structures played a
397 relatively minor role in the preserved deformation history of the STTFZ.

398

399 ***Mafic mylonites***

400 Mafic mylonite/ultramylonite shear zones do exist in the STTFZ but are very
401 rare, having been recognised only in the core of the western LFC (Murton 1986a).
402 They have previously assumed a significance greater than their abundance would merit
403 because many display clear sinistral shear sense, initially taken as evidence in support
404 of a sinistral shear sense for the transform fault as a whole (Murton 1986a). Broadly E-
405 W trending, they are typically only centimetres to a few decimetres wide, extremely

406 fine-grained and normally of greenschist (rarely amphibolite) facies. They are always
407 spatially associated with transform sequence gabbroic intrusions, in some cases
408 bounding parts of the plutons; significantly, most have mafic mineralogies within a
409 serpentinised peridotite country rock. MacLeod and Murton (1995) showed they
410 represent deformed remnants of transform sequence mafic dykes, and suggested the
411 sinistral shear sense represented the accommodation of small-scale localised clockwise
412 block rotations at the boundaries of intrusive bodies injected into the much broader
413 dextral (transform fault) shear zone. These mafic mylonites are of minor significance
414 and likely accumulated little strain within the STTFZ as a whole.

415

416 *Serpentinite shear zones*

417 Serpentinite shear zones are the principal transform-related structures in the
418 mantle section of the STTFZ, both in the western and northeastern parts of the LFC
419 (Figure 3). Whereas serpentinised peridotite is intensely deformed across most of the
420 LFC mantle sequence outcrop, distinct bands of more intense shearing have been
421 identified and are delineated in lime green in Figure 3. These discrete serpentinite
422 shear zones typically form E-W striking, vertical features; however, they may also
423 bound and juxtapose brittlely-deformed disrupted ocean crustal blocks inferred to have
424 formed at the Anti-Troodos ridge axis and then been incorporated into the broader
425 transform-tectonised zone.

426 Of the order of ~20 m wide on average, the serpentinite shear zones may
427 exceptionally be up to 500 m wide, may be traced ≥ 2 km along strike directly or
428 intermittently up to 8 km (Figure 3). They typically have poorly-defined boundaries
429 and are very heterogeneous in internal structure (Figures 4b, c). They are tectonic
430 mélanges, consisting of lenses ranging from centimetres to tens of metres in size and
431 phacoidal to rounded in shape, set in an intensely foliated matrix of scaly to schistose
432 serpentine of widely varying proportion (Figures 4b-d). Here, ‘scaly’ implies an
433 anastomosing network of discrete, curvilinear surfaces bounding relatively low strain
434 phacoids, whereas ‘schistose’ implies a subplanar, closely spaced (< cm), penetrative
435 foliation.

436 Serpentinite shear zones contain discrete slip surfaces subparallel to the scaly to
437 schistose fabric. S-C-C’ fabrics are common and display consistent dextral shear sense
438 on steeply dipping, E-W striking structures (MacLeod and Murton, 1995). The
439 proportion of matrix to clasts increases progressively with increased deformation

440 intensity, such that the highest strain serpentinite shear zones (mapped as lime green in
441 Figure 3) consist of broad zones of finely foliated schistose serpentinite containing
442 only isolated rounded clasts (Figure 4b-d). Clast lithology is principally harzburgite,
443 dunite or pyroxenite derived from the original mantle sequence host rock and
444 pervasively serpentinitised, but in many localities also includes blocks of wehrlite,
445 gabbro and dolerite from the transform intrusive suite. Many of the transform sequence
446 wehrlite intrusives are fresh, proving the early serpentinitisation of the mantle section.
447 Undeformed dolerite dykes may also cut the shear zones, attesting to the syn-tectonic
448 nature of the intrusions (Murton, 1986a; Gass et al., 1994). Mafic lithologies within
449 serpentinite are rodingitised in many instances, and in the shear zones the foliated
450 serpentinite adjacent to mafic blocks may also include tremolite. Talc has not been
451 found, though it may have been replaced during the 90 Myr exhumation history of the
452 LFC.

453

454 ***Brittle deformation of the mafic ocean crust***

455 Extensive brittle deformation has disrupted what is inferred to have originally
456 been a relatively regular ocean crustal section that was generated at an Anti-Troodos
457 ridge axis and incorporated into the STTFZ. As described above, much of the present-
458 day outcrop pattern of the crustal section, in the eastern LFC in particular, results from
459 extensional reactivation of the originally transform-parallel structures at the latest stage
460 of the seafloor history of the LFC. Nevertheless, the style of active transform fault
461 deformation within the mafic crust can be discerned both from the AFB and from the
462 variably disrupted blocks within the LFC.

463 Deformation is most clearly displayed within outcrops of the sheeted dyke
464 complex. Most such outcrops are brecciated to a greater or lesser degree across the
465 entire AFB and most of the northern LFC. The extent of disruption is commonly such
466 that dyke margins have been obliterated entirely on a scale of hundreds of metres or
467 more, and areas mapped as 'sheeted dyke complex' (Figure 3) are simply massive
468 dolerite fault breccia zones (Figure 4e, f). Belts of dolerite fault breccia have been
469 traced E-W for up to 7 km, and may be several hundreds of metres wide (MacLeod and
470 Murton, 1993). Sheeted dyke fault breccias are composed of unsorted angular to sub-
471 rounded fragments, with sub-millimetre to decimetre-sized, commonly polished clasts,
472 in what is normally a strongly indurated matrix (Figure 4e). Petrographic studies have
473 shown that breccia clasts are typically cemented by the same greenschist facies

474 background alteration that affects the clasts themselves (Simonian and Gass, 1978;
475 Gass et al., 1994). Disseminated sulphide mineralisation is common, which leads to
476 oxidation and characteristic red surface alteration of outcrops. Together these
477 observations show that pervasive flow of high-temperature fluids accompanied
478 deformation throughout the transform-tectonised zone.

479 Discrete fault planes and fault zones are widespread at all levels of the ocean
480 crust within the transform domain, though they are rarely well exposed. Their traces
481 can nevertheless be mapped out within the AFB and shown to have the form of a
482 braided anastomosing array on a scale of hundreds of metres (Figure 3; Simonian and
483 Gass, 1978; Gass et al., 1994). Within the transform valley these fault zones generated
484 an irregular seafloor of local transpressional highs and transtensional lows, the former
485 being eroded into the latter (see above; Simonian and Gass, 1978).

486 Whereas many of the sheeted dyke breccia zones within the AFB and northern
487 LFC are devoid of discrete fault planes, some faults do occur in association with the
488 breccia zones. In these instances localised (typically centimetre-scale) gouge and/or
489 foliated cataclasite may abut sub-planar fault surfaces that typically display low-angle
490 slickensides. These faults may also anastomose on a metre-scale, mimicking their
491 larger map-scale geometry.

492 Insights as to fault zone development and strain accommodation can be gained
493 from the regions of NE-SW dyke strike a few kilometres to the north and south of the
494 STTFZ itself. Within the regions affected by clockwise vertical-axis rotations
495 associated with drag at the transform inside corner (MacLeod et al., 1990), deformation
496 is also extensive but distributed on a metre- to tens-of-metres scale. Faults may either
497 be transform parallel, with a normal component of displacement stepping down
498 towards the AFB and northern LFC, or else dyke parallel. On the latter, low-angle
499 slickensides with minor sinistral offsets may be developed on individual dyke margins
500 in relatively low-strain lenses, surrounded by discrete surfaces with gouge and foliated
501 cataclasite passing into indurated breccia zones, together forming an anastomosing
502 zone of deformation distributed over a tens to hundreds of metre scale (Figure 4e).
503 Substantial variability in dyke margin orientations on this scale suggests that
504 significant rotational strains are associated with such deformation, fault breccia and
505 gouge being generated to accommodate local space problems. As within the STTFZ
506 itself, fault breccias within these dyke-parallel deformation zones tend to be strongly
507 indurated and associated with disseminated sulphide mineralisation. Mineralisation is

508 concentrated within the fault zones, demonstrating the strong link between fluid flow
509 and deformation.

510

511 **DISCUSSION: GEOLOGICAL CONTROLS ON TRANSFORM FAULT** 512 **SEISMICITY**

513 The observations described above highlight that transform faults comprise a
514 range of lithological units complexly juxtaposed in three dimensions within a
515 kilometres-wide fault zone. Although informative, conceptual models as shown in
516 Figure 1 are therefore simplistic in their 2-D nature, and also lack information on the
517 controls of locked vs. creeping vs. conditional frictional behaviour. Defining a
518 thermally controlled base to the seismogenic zone is also likely to be a simplification,
519 because variables such as composition and fluid pressure are inherently variable in
520 time and space, as shown by the observations in the STTFZ.

521

522 *Seismic style of basalts and sheeted dykes*

523 The STTFZ illustrates a layered nature, not clearly defined by the 600°C
524 isotherm, but more reasonably instead by the boundary between a disaggregated mafic
525 crust and serpentinised peridotite. Most clearly displayed in the sheeted dyke sequence,
526 the mafic crust deformed by a combination of discrete faults and distributed fracturing
527 (Figure 4g), leading to local development of broad breccia zones (Figure 4e, f). The
528 end-member deformation style of relatively intact dykes displaced by discrete faults,
529 typically developed along low-cohesion dyke margins, could be modelled as discrete
530 fault planes in an elastic medium. As the faults are in basalt (and dolerite and gabbro),
531 they are velocity-weakening at low temperatures of upper crustal deformation if they
532 can be approximated by olivine aggregates (Boettcher et al., 2007), and therefore likely
533 to create episodic earthquakes controlled by elastic loading. If fault strength and elastic
534 loading rates are constant, these earthquakes could be periodic.

535 Because earthquake magnitude depends on rupture area, the length of faults (or
536 soft-linked fault systems) and the thickness of the sheeted dyke section control the
537 maximum earthquake magnitude that can be hosted on faults developed along dyke
538 margins. These faults could, however, also propagate into underlying gabbro and upper
539 mantle if conditions and material properties allow. Assuming transform earthquakes
540 reflect elastic strain release with purely strike-slip displacement, the slip to length ratio
541 (u/L) of an earthquake rupture equals $\Delta\sigma/G$. The definitions of M and M_w can then be

542 combined and reorganised to express transform fault earthquake magnitude in terms of
543 stress drop and rupture geometry:

544

$$545 \quad 10^{3/2(M_w+6)} = M = GAu = GL^2W(\Delta\sigma/G) \quad (1)$$

546

547 where W is the downdip width of the rupture and L is along-strike length.

548 Estimates for the thickness of dyke complexes in ophiolites and modern
549 oceanic crust vary, both with uncertainty in data and interpretation, and between fast
550 and slow spreading centres (e.g. Christensen and Salisbury, 1975). However, 3 km is
551 near average, and is also the approximate combined thickness of lavas, dykes and
552 upper gabbros in Troodos (Christensen and Salisbury, 1975; Gass et al., 1994). Static
553 stress drop ($\Delta\sigma$) of transform fault earthquakes is typically ≤ 1 MPa (Boettcher and
554 Jordan, 2004). A typical shear modulus, G , of 30 GPa then yields $u/L = \Delta\sigma/G \leq 3 \times 10^{-5}$.
555 M_w 6.0 earthquakes like those on the Gofar transform have seismic moment of $\sim 10^{18}$
556 Nm, and would according to Eq. 1 then require a fault length of 19 km if constrained to
557 a 3 km depth interval, in Troodos restricted by the combined thickness of dykes, lavas,
558 and upper gabbros. This is consistent with observations by McGuire et al. (2012) who
559 define the rupture area of $\sim M_w$ 6 earthquakes as 15-20 km long and confined to a 3
560 km downdip width at 3-6 km depth. These depths are inferred to be above the Moho,
561 but may involve both sheeted dykes and underlying gabbroic rocks with similar
562 composition and properties.

563 The calculation above implies that crustal earthquakes in transform faults may
564 be constrained to slip surfaces within the dyke sequence, and possibly extensions into
565 overlying basalts and underlying dyke-bearing gabbro. The breccia zones within the
566 Troodos dyke sequence (Figure 4g), however, are more damaged and more porous, and
567 lack clear, through-going fault surfaces. It is also unclear how much elastic strain can
568 be accommodated in these rocks before failure. These zones may reflect the more
569 mature, more damaged, fault segments proposed to exist by Froment et al. (2014).
570 Shearing of a broad zone of poorly consolidated, granular material, as described in the
571 brecciated dyke complex in Troodos, would typically be strain hardening as shear
572 involves dilatancy, and therefore also velocity-strengthening and unlikely to fail in
573 earthquakes (Marone et al., 1990). This would be consistent with damaged crustal

574 zones separating locked patches in the Gofar transform (McGuire et al., 2012; Froment
575 et al., 2014).

576

577 *Seismic style of mantle rocks*

578 The almost complete absence of evidence of high-temperature deformation of
579 peridotite in the STTFZ is striking. The exposed mantle rocks are near pervasively
580 serpentinitised, and strain was accommodated almost completely by deformation of
581 serpentinite. These observations demonstrate that penetration of water deep into the
582 mantle lithosphere was efficient and widespread within the active transform domain.

583 One can envisage the serpentinitisation to be a time- and strain-dependent
584 process, implying an interplay in which increased serpentinitisation allows strain
585 localisation that in turn leads to dilation, fluid infiltration, and further increased
586 serpentinitisation. As such, serpentinite shear zones are likely to be strain-weakening on
587 geological time scales. Such interplay between fluid flow, serpentinitisation, and
588 deformation has been investigated in several settings (e.g. Escartin et al., 1997; Pérez-
589 Gussinyé and Reston, 2001; Wada et al., 2008; Hirth and Guillot, 2013) but warrants
590 further exploration in the case of oceanic transform faults.

591 An important conclusion is that the controlling rheology throughout the mantle
592 lithosphere within the STTFZ is serpentine, not olivine-rich peridotite; thus the
593 controlling parameters must be those that control the behaviour of serpentinite,
594 including the volumetric proportion and distribution of serpentine minerals.

595 One note of caution against over-interpreting the importance of serpentine,
596 however, is that peridotite mylonites have been sampled from oceanic fracture zones
597 (e.g. Jaroslow et al., 1996). Warren and Hirth (2006) have, accordingly, suggested that
598 mylonitisation, grain size reduction, and a transition to diffusion creep in peridotite can
599 lead to weakening along transforms. It is therefore likely that ductile lithosphere at
600 deep levels within active transform zones can also deform by distributed flow of
601 peridotite. This is probably the case in areas near the base of the lithosphere that are
602 above the upper temperature stability limit of serpentine, as Warren and Hirth (2006)
603 interpret mylonitisation and strain weakening to have occurred in the absence of water,
604 with a small grain size maintained by pinning.

605 A similar mechanism may be recorded by the foliated peridotites in Troodos
606 (Figure 4a); note, however, that these shear zones are narrow, poorly preserved, and
607 played a minor role in accommodating strain along the dominant mapped structures

608 within the STTFZ. Peridotite mylonites in the mantle section are typically cross-cut
609 and obliterated by the abundant serpentinite shear zones. It is therefore likely that the
610 deep extension of transforms creep steadily by diffusion creep in peridotite until
611 damage and downward propagation of brittle faults allow hydration and
612 serpentinisation. Water penetration, cooling and embrittlement of the STTFZ must
613 therefore have occurred almost to the base of the lithosphere within the active
614 transform fault zone, similar to that at the base of many oceanic detachment faults
615 (MacLeod et al., 2002, Escartin et al., 2003). This interpretation is consistent with
616 deeper seismicity along fault zones interpreted as more porous and damaged on
617 transforms along the East Pacific Rise (to as much as 10 km below seafloor; e.g.
618 McGuire, 2012; Froment et al., 2014; Wolfson-Schwehr et al., 2014).

619 A parameter that determines the strength and behaviour of the mantle and lower
620 crust is therefore the degree of alteration, likely controlled by fluid flow paths and
621 temperature. If fluids predominantly originate at the seafloor and percolate down,
622 serpentine shear zones are likely down-dip continuations of faults within the overlying
623 dyke sequence, controlled by fluid flow along these faults. If fluids have a deeper
624 source, e.g. magmatic systems on leaky transforms, then new shear zones may initiate
625 at depth, and their deformation control the location of overlying faults. In either case, it
626 is likely that serpentine shear zones connect to faults in the overlying sheeted dyke
627 complex. If this interpretation is correct, then rate-dependent behaviour of serpentine
628 may determine whether earthquakes in the crust can propagate downwards. Similarly,
629 serpentine frictional properties may determine whether earthquakes can initiate in the
630 upper mantle, and potentially propagate to velocity-weakening fault rock assemblages
631 at shallower levels.

632

633 *Seismic Style of Serpentinite Shear Zones*

634 Serpentine is likely to be present in the form of lizardite or chrysotile at
635 low (<300°C) temperatures, whereas the higher temperature phase antigorite is
636 prevalent at more than 300°C (Evans et al., 1976). At room temperature, antigorite has
637 a frictional coefficient in excess of 0.5 and is not significantly weaker than other non-
638 serpentine minerals (Reinen et al., 1994). However, with increasing temperature,
639 antigorite friction decreases, to as low as 0.1 at temperatures >400°C (Chernak and
640 Hirth, 2010). Both lizardite and antigorite have shown a transition from velocity-
641 strengthening at low velocities to velocity-weakening at high velocities (Reinen et al.,

642 1994). Accordingly, serpentinite shear zones are likely to accommodate stable creep
643 under steady-state conditions. This interpretation is supported by studies of serpentinite
644 schistosity in the Santa Ynez fault of the San Andreas system, where microstructures
645 imply mineral growth by a dissolution-precipitation mechanism at slow strain rates
646 (Andreani et al., 2005).

647 Although generally aseismic and stably sliding at low velocities there is a
648 possibility of unstable behaviour in serpentinite if velocity increases. The room
649 temperature experiments of Reinen et al. (1994) implied that both lizardite and
650 antigorite faults are unable to nucleate earthquakes, but can allow earthquake
651 propagation as their behaviour becomes unstable at high velocities. At higher
652 temperatures, Chernak and Hirth (2010) have shown a general velocity-strengthening
653 behaviour of antigorite, and inferred that high temperature deformation of serpentine is
654 likely to occur by steady creep. Kohli et al. (2011), however, demonstrated that
655 dynamic weakening at near-seismic velocities can occur if slip is fast relative to
656 thermal diffusion, allowing flash heating at ambient temperatures as low as 300°C if
657 velocity is high and slip is localised.

658 The range of strain rate dependent behaviours of serpentine outlined above
659 emphasises that under most conditions, serpentinite shear zones are capable of
660 accommodating steady creep at low shear stress. However, depending on variables
661 including temperature, normal stress, fluid pressure, and deforming thickness, a range
662 of behaviours can occur if velocity increases (e.g. Hirth and Guillot, 2013). The
663 efficiency of steady creep is also dependent on the proportion of serpentine, as
664 serpentine shear zones form progressively through alteration of olivine-rich
665 assemblages and are typically preserved as *mélanges* of foliated serpentine with
666 peridotite clasts (Figure 4b-d). As little as 9% serpentine may lower the strength of the
667 aggregate to that of pure serpentine (Escartin et al., 2001). We observe that peridotite
668 clasts within shear zones in the STTFZ are serpentinised although they lack the foliated
669 structure of the surrounding matrix; therefore, serpentine shear zones are likely to be
670 weak, even when clast dominated, but can still only control deformation if
671 interconnected. Oceanic transform-related serpentine shear zones are yet to be
672 described in detail over a range of scales. We do, however, speculate that a mechanism
673 to create locked zones within creeping upper mantle is to have fault volumes where
674 serpentinisation is incomplete. In such volumes, interseismically locked zones could
675 represent lack of interconnected serpentine, or less alignment of serpentine crystals,

676 and not be able to creep at plate boundary deformation rates. These zones would
677 therefore be loaded by surrounding creep, and eventually fail as local stress reach a
678 failure criterion (Sibson, 1980; Handy, 1990). When this happens, surrounding,
679 creeping rocks are either going to arrest slip or be conditionally stable, depending on
680 composition, temperature, fluid pressure, and other parameters. In the latter case, slip
681 may propagate at seismic rate.

682

683 **CONCLUSIONS**

684 The exhumed STTFZ is an ~5 km wide tabular zone comprised of abundant
685 sheared serpentinite mélanges overprinting rare foliated peridotites at lithospheric
686 mantle levels, contrasting with discrete faults and broad zones of breccias within
687 mafic, mostly doleritic, crustal level rocks. The range of rock types and the complex
688 way in which they are juxtaposed reflects a range of deformation modes and would
689 have generated a heterogeneous style of seismicity. We suggest that the internal
690 structure of modern oceanic transform faults will be broadly comparable to that of the
691 STTFZ, and hence that the seismic style of modern oceanic transforms (Figure 1) is
692 likely to result from similar geological complexity across a range of scales.

693 Deformation in the crustal sequence contains two end-members: broad breccias
694 (Figure 4e, f) and discrete faults (Figure 4g). We hypothesise that these represent
695 aseismic and seismic deformation, respectively: although basaltic rocks are velocity
696 weakening at crustal temperatures, distributed shear through a poorly consolidated
697 breccia is likely to be velocity-hardening because of dilatancy. We propose that an
698 explanation for the spatially distinct rupture areas in active transforms is that they are
699 bounded by broad breccia zones through which slip cannot propagate at seismic rates
700 (Figure 1b). Observations in the Charlie-Gibbs transform (McGuire et al., 2012) have
701 suggested that creeping segments can be conditionally stable (Figure 1d), which could
702 be possible in the above interpretation if the breccias are fluid over-pressured or
703 sufficiently cemented to host local, discrete slip zones.

704 Deformation in the mantle is largely accommodated in serpentinite shear zones.
705 These zones would typically deform by steady creep, but can host seismic slip under
706 conditions where fast slip is sufficiently localised. Rare, locally preserved, foliated
707 upper mantle peridotites (Figure 4a) attest to ductile, likely transform related shearing
708 also in mantle rocks, possibly under dry conditions before fluids reached mantle depths
709 and allowed serpentinisation.

710 These observations and inferences imply that transform fault seismicity
711 depends on time- and strain- and permeability-dependent processes. Future projects
712 that combine detailed, high-resolution passive- and active-source seismology with high
713 resolution mapping and sampling will be necessary to refine our models and
714 hypotheses. Further field investigations of exhumed transforms are also essential to
715 better characterise the structures, deformation mechanisms, and compositions involved
716 in the various styles of deformation that we document here.

717

718 **ACKNOWLEDGMENTS**

719 We acknowledge with gratitude the Director and staff of the Geological Survey
720 Department of Cyprus for permission to work in Cyprus and for their ongoing support.
721 We thank Bram Murton, Joe Cann and many others for helping us refine our ideas over
722 many years, and Joao Duarte for his encouragement and patience. A. F. is supported by
723 the European Research Council (ERC) grant agreement 715836 “MICA”.

724

725 **REFERENCES**

- 726 Abercrombie, R.E. and Ekström, G. (2001). Earthquake slip on oceanic transform
727 faults. *Nature* 410, 74-77.
- 728 Aderhold, K., and Abercrombie, R.E. (2016). The 2015 Mw 7.1 earthquake on the
729 Charlie - Gibbs transform fault: Repeating earthquakes and multimodal slip on a
730 slow oceanic transform. *Geophys. Res. Lett.* 43, 6119-6128.
- 731 Allerton, S. and Vine, F.J. (1990). Palaeomagnetic and structural studies of the
732 southeastern part of the Troodos complex. In: Malpas, J.; Moores, E.M.;
733 Panayiotou, A. and Xenophontos, C. (eds.) *Ophiolites: Oceanic Crustal*
734 *Analogues, Proceedings of the Symposium “Troodos 87: Ophiolites and oceanic*
735 *lithosphere”* (pp. 99-111) Geological Survey Department, Nicosia, Cyprus.
- 736 Andreani, M., Boullier, A.-M. and Gratier, J.-P. (2005). Development of schistosity by
737 dissolution-crystallization in a Californian serpentinite gouge. *J. Struct. Geol.* 27,
738 2256-2267.
- 739 Bird, P., Kagan, Y.Y. and Jackson, D.D. (2002). Plate tectonics and earthquake
740 potential of spreading ridges and oceanic transform faults. In Stein, S. and
741 Freymuller, J.T. (Eds.), *Plate Boundary Zones*. Geodyn.Ser. v. 30, pp. 203-218.
742 AGU: Washington D.C.

743 Bird, P., and Kagan, Y.Y. (2004). Plate-tectonic analysis of shallow seismicity:
744 Apparent boundary width, beta, corner magnitude, coupled lithosphere thickness,
745 and coupling in seven tectonic settings. *Bull. Seismol. Soc. America*, 94, 2380-
746 2399.

747 Boettcher, M.S. and Jordan, T.H. (2004). Earthquake scaling relations for mid-ocean
748 ridge transform faults. *J. Geophys. Res.* 109, B12302.

749 Boettcher, M.S., Hirth, G. and Evans, B. (2007). Olivine friction at the base of oceanic
750 seismogenic zones. *J. Geophys. Res.* 112, B01205.

751 Bonatti, E. and Honnorez, J. (1976). Sections of the earth's crust in the equatorial
752 Atlantic. *J. Geophys. Res.* 81, 4104-4116.

753 Bonhommet, N., Roperch, P. and Calza, F. (1988). Palaeomagnetic arguments for
754 block rotations along the Arakapas fault (Cyprus). *Geology* 16, 422-425.

755 Braunmiller, J. and Nábělek, J. (2008). Segmentation of the Blanco Transform Fault
756 Zone from earthquake analysis: Complex tectonics of an oceanic transform fault.
757 *J. Geophys. Res.* 113, B07108.

758 Brune, J.N. (1968). Seismic moment, seismicity, and rate of slip along major fault
759 zones. *J. Geophys. Res.* 73, 777-784.

760 Cann J.R., Prichard H.M., Malpas J.G. and Xenophontos C. (2001). Oceanic inside
761 corner detachments of the Limassol Forest area, Troodos ophiolite, Cyprus. *J.*
762 *Geol. Soc. London* 158, 757-767.

763 Ceuleneer, G., Nicolas, A. and Boudier, F. (1988). Mantle flow patterns at an oceanic
764 spreading centre: the Oman peridotites record. *Tectonophysics*. 151, 1-26.

765 Chernak, L.J. and Hirth, G. (2010). Deformation of antigorite serpentinite at high
766 temperature and pressure. *Earth Planet. Sci. Lett.* 296, 23-33.

767 Christensen, N.I. and Salisbury, M.H. (1975). Structure and constitution of the lower
768 oceanic crust. *Rev. Geophys.* 13, 57-86.

769 Collettini, C., Niemeijer, A., Viti, C., Smith, S.A. and Marone, C. (2011). Fault
770 structure, frictional properties and mixed-mode fault slip behavior. *Earth Planet.*
771 *Sci. Lett.* 311, 316-327.

772 Dieterich, J.H. (1992). Earthquake nucleation on faults with rate-and state-dependent
773 strength. *Tectonophysics* 211, 115-134.

774 Embley, R.W., Wilson, D.S. (1992). Morphology of the Blanco Transform Fault Zone-
775 NE Pacific: Implications for its tectonic evolution. *Marine Geophysical*
776 *Researches* 14, 25-45.

777 Escartin, J., Hirth, G. and Evans, B. (1997). Effects of serpentization on the
778 lithospheric strength and the style of normal faulting at slow-spreading ridges.
779 *Earth Planet. Sci. Lett.* *151*, 181-189.

780 Escartin, J., Hirth, G., and Evans, B. (2001). Strength of slightly serpentized
781 peridotites: Implications for the tectonics of oceanic lithosphere. *Geology* *29*,
782 1023-1026.

783 Escartín, J., Mével, C., MacLeod, C.J. and McCaig, A.M. (2003). Constraints on
784 deformation conditions and the origin of oceanic detachments: the Mid-Atlantic
785 Ridge core complex at 15°45'N. *Geochem., Geophys., Geosys.* *4* (8),
786 doi:10.1029/2002GC000472, 37pp.

787 Evans, B.W., Johannes, H., Oterdoom, H. and Trommsdorff, V. (1976). Stability of
788 chrysotile and antigorite in the serpentine multisystem. *Schweiz. Miner. Petrogr.*
789 *Mitt.* *56*, 79-93.

790 Fagereng, Å., and Sibson, R. H. (2010). Melange rheology and seismic style. *Geology*
791 *38*, 751-754.

792 Fox, P.J. and Gallo, D.G. (1984). A tectonic model for ridge-transform-ridge plate
793 boundaries: Implications for the structure of oceanic lithosphere. *Tectonophysics*
794 *104*, 205-242.

795 Froment, B., McGuire, J.J., Hilst, R.D., Gouédard, P., Roland, E.C., Zhang, H. and
796 Collins, J.A. (2014). Imaging along-strike variations in mechanical properties of
797 the Gofar transform fault, East Pacific Rise. *J. Geophys. Res.* *119*, 7175-7194.

798 Gass, I.G., MacLeod, C.J., Murton, B.J., Panayiotou, A., Simonian, K.O. and
799 Xenophontos, C. (1994). *The Geological Evolution of the Southern Troodos*
800 *Transform Fault Zone*. Cyprus Geological Survey Memoir, **9**, Geological Survey
801 Dept., Nicosia, Cyprus, 218pp.

802 Gass, I.G. and Masson-Smith, D. (1963). The Geology and Gravity Anomalies of the
803 Troodos Massif, Cyprus, *Phil. Trans. Roy. Soc. London A255*, 417-467.

804 Handy, M.R. (1990). The solid-state flow of polymineralic rocks. *J. Geophys. Res.* *95*,
805 8647-8661.

806 Hékinian, R., Bideau, D., Hébert, R., and Niu, Y. (1995). Magmatism in the Garrett
807 transform fault (East Pacific Rise near 13°27'S). *J. Geophys. Res.* *100*, 10163–
808 10185.

809 Hirth, G. and Guillot, S. (2013) Rheology and tectonic significance of serpentinite.
810 *Elements* *9*, 107-113.

811 Honnorez, J., Mével, C., and Montigny, R. (1984). Geotectonic significance of gneissic
812 amphibolites from the Vema fracture zone, Equatorial Mid-Atlantic Ridge. *J.*
813 *Geophys. Res.* 89, 11379-11400.

814 Ide, S., Baltay, A. and Beroza, G.C. (2011). Shallow dynamic overshoot and energetic
815 deep rupture in the 2011 Mw 9.0 Tohoku-Oki earthquake. *Science* 33, 1426-1429.

816 Jaroslaw, G.E., Hirth, G. and Dick, H.J.B. (1996). Abyssal peridotite mylonites:
817 implications for grain-size sensitive flow and strain localization in the oceanic
818 lithosphere. *Tectonophysics* 256, 17-37.

819 Karson, J.A. and H.J.B. Dick (1983). Tectonics of ridge-transform intersections at the
820 Kane Fracture Zone, 24°N on the Mid-Atlantic Ridge. *Mar. Geophys. Res.* 6, 51-
821 98.

822 Kohli, A.H., Goldsby, D.L., Hirth, G. and Tullis, T. (2011). Flash weakening of
823 serpentinite at near-seismic slip rates. *J. Geophys. Res.* 116, B03202.

824 Lay, T. and Kanamori, H. (1981) An asperity model of large earthquake sequences. In:
825 *Earthquake Prediction*. Maurice Ewing Series. No.4. American Geophysical
826 Union, pp. 579-592. ISBN 9780875904030.

827 Macdonald, K.C., Castillo, D.A., Miller, S.P., Fox, P.J., Kastens, K.A. and Bonatti, E.
828 (1986). Deep - tow studies of the Vema Fracture Zone: 1. Tectonics of a major
829 slow slipping transform fault and its intersection with the Mid-Atlantic Ridge. *J.*
830 *Geophys. Res.* 91, 3334–3354.

831 MacLeod, C.J. (1988). *The tectonic evolution of the Eastern Limassol Forest Complex,*
832 *Cyprus*. Unpubl. PhD thesis, Open University, 231pp.

833 MacLeod, C.J. (1990). Role of the Southern Troodos Troodos Transform Fault in the
834 rotation of the Cyprus microplate: evidence from the Eastern Limassol Forest
835 Complex. In: Malpas, J.; Moores, E.M.; Panayiotou, A. and Xenophontos, C.
836 (eds.) *Ophiolites: Oceanic Crustal Analogues, Proceedings of the Symposium*
837 *“Troodos 87: Ophiolites and oceanic lithosphere”* (pp. 75-85) Geological Survey
838 Department, Nicosia, Cyprus.

839 MacLeod, C.J., Allerton, S., Gass, I.G. and Xenophontos, C. (1990). Structure of a
840 fossil ridge-transform intersection in the Troodos ophiolite. *Nature* 348, 717-720.

841 MacLeod, C.J., Escartín, J., Banerji, D., Banks, G.J., Gleeson, M., Irving, D.H.B.,
842 Lilly, R.M., McCaig, A.M., Niu, Y., Allerton, S., and Smith, D.K. (2002). Direct

843 geological evidence for oceanic detachment faulting: the Mid-Atlantic Ridge,
844 15°45'N *Geology* 30, 879–882.

845 MacLeod, C.J. and Murton, B.J. (1993). Structure and tectonic evolution of the
846 Southern Troodos Transform Fault Zone, Cyprus. In: Prichard, H.M., Alabaster,
847 T., Harris, N.B. and Neary, C.R. (eds.) *Magmatic Processes and Plate Tectonics*
848 (pp. 141-176) Geological Society London Special Publication No. 76.

849 MacLeod, C.J. and Murton, B.J. (1995). On the sense of slip of the Southern Troodos
850 transform fault zone, Cyprus. *Geology* 23, 257-260.

851 Marone, C., Raleigh, C.B. and Scholz, C. (1990). Frictional behavior and constitutive
852 modelling of simulated fault gouge. *J. Geophys. Res.* 95, 7007–7025.

853 McGuire, J.J., Boettcher, M.S. and Jordan, T.H. (2005). Foreshock sequences and
854 short-term earthquake predictability on East Pacific Rise transform faults. *Nature*
855 434, 457-461.

856 McGuire, J.J., Collins, J.A., Gouédard, P., Roland, E., Lizarralde, D., Boettcher, M.S.,
857 Behn, M.D. and Van Der Hilst, R. D. (2012). Variations in earthquake rupture
858 properties along the Gofar transform fault, East Pacific Rise. *Nature Geoscience* 5,
859 336-341.

860 McKenzie, D.P., Jackson, J. and Priestly, K. (2005). Thermal structure of oceanic and
861 continental lithosphere. *Earth Planet. Sci. Lett.* 233, 337-349.

862 Molnar, P., Atwater, T., Mammerickx, J., & Smith, S. M. (1975). Magnetic anomalies,
863 bathymetry and the tectonic evolution of the South Pacific since the Late
864 Cretaceous. *Geophys. J. Int.* 40, 383-420.

865 Moore, D. E., D. A. Lockner, S. Ma, R. Summers, and J. D. Byerlee (1997), Strengths
866 of serpentinite gouges at elevated temperatures, *J. Geophys. Res.*, 102, 14787–
867 14801.

868 Moores, E.M., Varga, R.J., Verosub, K.L. and Ramsden, T.W. (1990). Regional
869 structure of the Troodos dyke complex. In: Malpas, J.; Moores, E.M.; Panayiotou,
870 A. and Xenophontos, C. (eds.) *Ophiolites: Oceanic Crustal Analogues,*
871 *Proceedings of the Symposium “Troodos 87: Ophiolites and oceanic lithosphere”*
872 (pp. 27-35) Geological Survey Department, Nicosia, Cyprus.

873 Moores, E.M. and Vine, F.J. (1971). The Troodos Massif, Cyprus and other ophiolites
874 as oceanic crust: evaluation and implications. *Phil. Trans. Roy. Soc., Lond.* 268,
875 443-466.

876 Morris, A., Creer, K.M. and Robertson, A.H.F. (1990). Palaeomagnetic evidence for
877 clockwise rotations related to dextral shear along the Southern Troodos Transform
878 Fault (Cyprus). *Earth Planet. Sci. Lett.* 99, 250-262, 1990.

879 Mukasa, S.B. and Ludden, J.N. (1987). Uranium-lead isotopic ages of plagiogranites
880 from the Troodos ophiolite, Cyprus, and their tectonic significance. *Geology* 15,
881 825-828.

882 Murton, B.J. (1986a). Anomalous oceanic lithosphere formed in a leaky transform
883 fault: evidence from the Western Limassol Forest Complex, Cyprus. *J. Geol. Soc.*
884 *London* 143, 845-854.

885 Murton, B.J. (1986b). *The tectonic evolution of the Western Limassol Forest Complex,*
886 *Cyprus*. Unpubl. PhD thesis, Open University, 332pp.

887 Nicolas, A. and Poirier, J.P. (1976). *Crystalline plasticity and solid state flow in*
888 *metamorphic rocks*. Wiley, New York, 444pp.

889 Noda, H. and Lapusta, N. (2013). Stable creeping fault segments can become
890 destructive as a result of dynamic weakening. *Nature* 493, 518-521.

891 Pérez-Gussinyé, M. and Reston, T.J. (2001). Rheological evolution during extension at
892 nonvolcanic rifted margins: onset of serpentinization and development of
893 detachments leading to continental breakup. *J. Geophys. Res.* 106, 3961-3975.

894 Pockalny, R.A., Detrick, R.S. and P. J. Fox (1988). Morphology and tectonics of the
895 Kane Transform from Sea Beam bathymetry data. *J. Geophys. Res.* 93, 3179–
896 3193.

897 Prinz, M., Keil, K., Green, J.A., Reid, A.M., Bonatti, E. and Honnorez, J. (1976).
898 Ultramafic and mafic samples from the equatorial Mid-Atlantic Ridge and fracture
899 zones. *J. Geophys. Res.* 81, 4087-4103.

900 Reinen, L.A., Weeks, J.D. and Tullis, T.E. (1994). The frictional behavior of lizardite
901 and antigorite serpentinites: Experiments, constitutive models, and implications
902 for natural faults. *Pure Appl. Geophys.* 143, 317-358.

903 Robertson, A.H.F., Parlak, O. and Ustaömer, T. (2012). Overview of the Palaeozoic–
904 Neogene evolution of Neotethys in the Eastern Mediterranean region (southern
905 Turkey, Cyprus, Syria). *Petrol. Geosci.* 18, 381-404.

906 Roland, E., Lizarralde, D., McGuire, J.J. and Collins, J.A. (2012). Seismic velocity
907 constraints on the material properties that control earthquake behavior at the
908 Quebrada-Discovery-Gofar transform faults, East Pacific Rise. *J. Geophys. Res.*
909 117, B11102.

910 Scholz, C. H. (1998). Earthquakes and friction laws. *Nature* 391, 37-42.

911 Scott, C.P., Titus, S.J. and Davis J.R. (2013). Using field data to constrain a numerical
912 kinematic model for ridge-transform deformation in the Troodos ophiolite,
913 Cyprus. *Lithosphere* 5, 109-127.

914 Searle, R.C. (1981). The Active Part of the Charlie Gibbs Fracture Zone: A Study
915 Using Sonar and Other Geophysical Techniques. *J. Geophys. Res.* 86, 243–262.

916 Searle, R. C. (1983). Multiple, Closely-Spaced Transform Faults in Fast-Slipping
917 Fracture Zones. *Geology* 11, 607–610.

918 Segall, P., Rubin, A.M., Bradley, A.M. and Rice, J.R. (2010). Dilatant strengthening as
919 a mechanism for slow slip events. *J. Geophys. Res.* 115, B12305.

920 Segall, P. and Rice, J. R. (1995). Dilatancy, compaction, and slip instability of a fluid-
921 infiltrated fault. *J. Geophys. Res.* 100, 22155-22171.

922 Sibson, R.H. (1980). Transient discontinuities in ductile shear zones. *J. Struct. Geol.* 2,
923 165-171.

924 Simonian, K.O. (1975). *The geology of the Arakapas Fault Belt area, Troodos*
925 *ophiolite, Cyprus*. Unpubl. PhD thesis, Open University, 151pp.

926 Simonian, K.O. and Gass, I.G. (1978). Arakapas fault belt, Cyprus: A fossil transform
927 fault. *Geol. Soc. America Bulletin* 89, 1220–1230.

928 Simons, M., Minson, S.E., Sladen, A., Ortega, F., Jiang, J., Owen, S.E., Meng, L.,
929 Ampuero, J.-P., Wei, S., Chu, R., Helmberger, D.V., Kanamori, H., Hetland, E.,
930 Moore, A.W. and Webb, F.H. (2011). The 2011 magnitude 9.0 Tohoku-Oki
931 earthquake: Mosaicking the megathrust from seconds to centuries. *Science* 332,
932 1421-1425.

933 Stewart, L.M. and Okal, E. A. (1983). Seismicity and aseismic slip along the Eltanin
934 Fracture Zone. *J. Geophys. Res.* 88, 10495-10507.

935 Sykes, L.R. and Ekström, G. (2012). Earthquakes along Eltanin transform system, SE
936 Pacific Ocean: Fault segments characterized by strong and poor seismic coupling
937 and implications for long-term earthquake prediction. *Geophys. J. Int.* 188, 421-
938 434.

939 Varga, R.J. and Moores, E.M. (1985). Spreading structure of the Troodos ophiolite,
940 Cyprus. *Geology* 13, 846-850.

941 Wada, I., Wang, K., He, J. and Hyndman, R.D. (2008). Weakening of the subduction
942 interface and its effects on surface heat flow, slab dehydration, and mantle wedge
943 serpentization. *J. Geophys. Res.* 113, B04402.

944 Wang, K., and Dixon, T. (2004), “Coupling” Semantics and science in earthquake
945 research, *Eos Trans. AGU*, 85(18), 180–180.

946 Warren, J.M. and Hirth, J.G. (2006). Grain size sensitive deformation mechanisms in
947 naturally deformed peridotites. *Earth Planet. Sci. Lett.* 248, 423-435.

948 Wells, D.L., and Coppersmith, K.J. (1994). New empirical relationships among
949 magnitude, rupture length, rupture width, rupture area, and surface displacement.
950 *Bull. Seismol. Soc. America* 84, 974-1002.

951 Wesnousky, S.G. (2006). Predicting the endpoints of earthquake ruptures. *Nature* 444,
952 358-360.

953 Wessel, P. and Haxby, W.F. (1990). Thermal stresses, differential subsidence, and
954 flexure at oceanic fracture zones. *J. Geophys. Res.* 95, 375-391.

955 Wessel, P.W. Smith, H.F., Scharroo, R., Luis, J. and Wobbe, F. (2013). Generic
956 Mapping Tools: Improved Version Released, *EOS Trans. AGU* 94, 409-410.

957 Wolfson-Schwehr, M., Boettcher, M.S., McGuire, J.J. and Collins, J.A. (2014). The
958 relationship between seismicity and fault structure on the Discovery transform
959 fault, East Pacific Rise. *Geochem., Geophys., Geosystems* 15, 3698-3712.

960 Zweck, C., Freymueller, J.T., and Cohen, S.C. (2002). Three-dimensional elastic
961 dislocation modeling of the postseismic response to the 1964 Alaska earthquake. *J.*
962 *Geophys. Res.* 107, doi: 10.1029/2001JB000409.

963

964 **FIGURE CAPTIONS**

965

966 Figure 1. Panel (a) shows the geometry and seismicity of the East Pacific Rise
967 Transform faults, highlighting locked patches producing M_w 6 or greater earthquakes
968 on the Gofar transform (patches as defined by Froment et al., 2014). Panel b) is a
969 schematic illustration of how a ‘single mode’ model may explain the distribution of
970 seismicity on the Gofar transform, following interpretations by McGuire et al. (2012).
971 Panel (c) shows the geometry and seismicity of the Charlie-Gibbs transform,
972 highlighting epicentres of repeating large earthquakes (after Aderhold and
973 Abercrombie, 2016). Panel (d) depicts the ‘multi-mode’ model that may describe the
974 frictional properties of a fault that fails in large earthquakes emanating from locked
975 patches that are smaller than their rupture areas (based on descriptions and
976 interpretations by Boettcher and Jordan (2004) and Aderhold and Abercrombie
977 (2016)). Panels (a) and (c) were produced using Generic Mapping Tools (Wessel et al.,
978 2013), seismic data from the ANSS database (including earthquakes $\geq M_w$ 4.0 from
979 1964 to 2014), and bathymetry from the GEBCO_2014 Grid, version 20150318,
980 www.gebco.net.

981

982 Figure 2. Outline geological map of the Troodos ophiolite, Cyprus. The Solea graben is
983 an ocean-floor extensional feature interpreted as an abandoned spreading centre. The
984 Southern Troodos Transform Fault Zone is an E-W dextral strike-slip fault zone
985 perpendicular to the overall N-S trend of sheeted dykes. Curvature of dyke orientations
986 north of the transform reflects clockwise rotations, inferred to reflect drag at the inside
987 corner of a ridge-transform intersection.

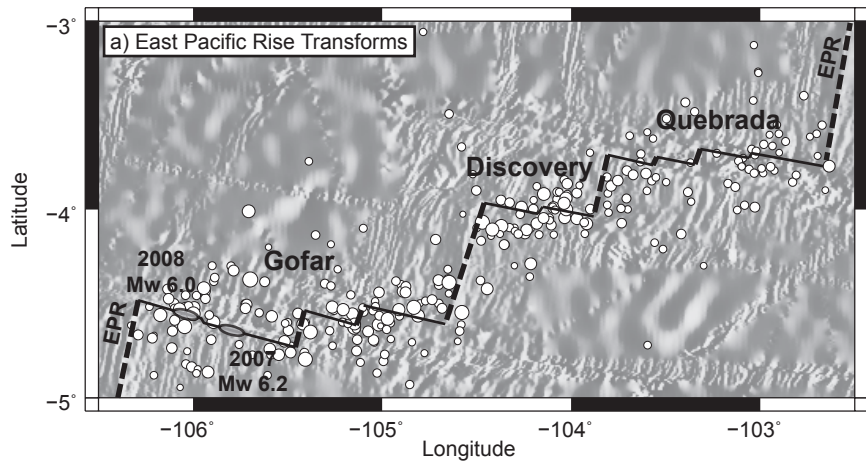
988

989 Figure 3. (a): Geological map of the Limassol Forest Complex, showing approximate
990 limits of the Southern Troodos Transform Fault Zone and Anti-Troodos domain, after
991 Gass et al. (1994). AFB = Arakapas Fault Belt. (b): Inset map showing detail of the
992 scale of geological complexity within the Southern Troodos Transform Fault Zone,
993 documented from original 1:5000 scale mapping by Simonian (1975), Murton (1986a)
994 and MacLeod (1988).

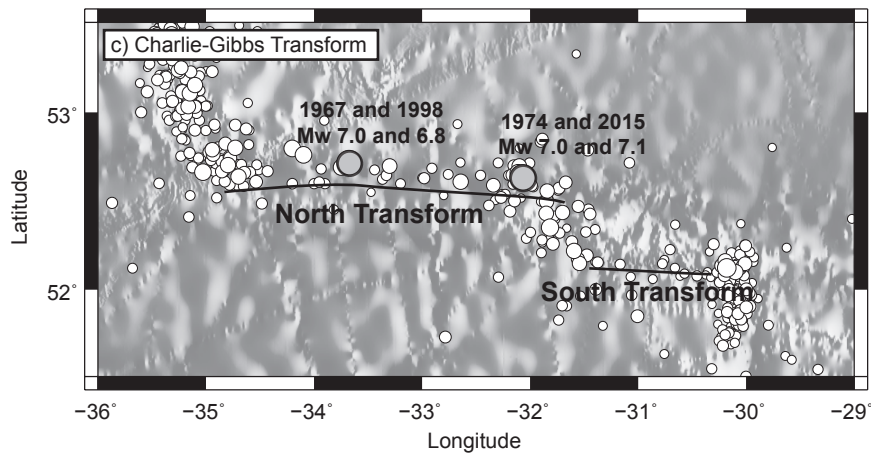
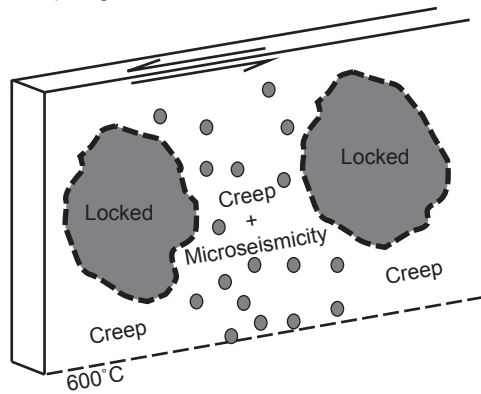
995

996 Figure 4. (a): Well foliated E-W trending porphyroclastic fabric in peridotite, now
997 serpentinitised. Such shear zones represent the only surviving evidence for transform-

998 related ductile deformation in the peridotites. (b), (c) and (d): Serpentinite shear zones,
999 showing heterogeneous nature of fabrics. The proportion of fine scaly matrix is
1000 greatest in the inferred highest strain zones (d). Such serpentinite shear zones are the
1001 dominant mode of deformation in the mantle section of the transform zone. (e), (f):
1002 Dolerite fault breccias derived from the sheeted dyke complex. Broad E-W trending
1003 belts of fault breccia are the predominant mode of deformation in the mafic ocean
1004 crustal section within the transform-tectonised zone. (g): Typical mode of deformation
1005 of sheeted dyke complex in the region 1-2 km north and south of the transform zone.
1006 Anastomosing bands of gouge and fault breccia (right) surround less deformed sheeted
1007 dykes (left). Flow of high-temperature fluids through the system gives rise to
1008 disseminated sulphide mineralisation (orange).



b) Single Mode Model



d) Multi-Mode Model

